

# ITERATIVELY REWEIGHTED DESIGN OF OVERSAMPLING COMPLEX-MODULATED FILTER-BANKS FOR HIGH OUTPUT-SIGNAL QUALITY

Thomas Kurbiel and Daniel Alfsmann and Heinz G. Gockler

Digital Signal Processing Group (DISPO), Ruhr-Universität Bochum, 44780 Bochum, Germany  
phone: +49 234 32 22106, fax: +49 234 32 02106, email: {kurbiel,alfsmann,goeckler}@nt.rub.de, web: www.dsv.rub.de

## ABSTRACT

This paper addresses the improvement of the signal-to-disturbance ratio of the output-signal of an oversampling, complex-modulated subband-coder filter-bank pair with extensive subband-signal amplification. The undesired non-linear disturbance is induced by the sample rate conversion within the filter-bank pair and it is hard to predict in dependence of the signal amplification. This has not been considered in most current design methods, leading to high prototype filter lengths in order to obtain desired signal-to-disturbance ratios.

In this paper, we propose a formulation for the design of a filter-bank which is based on the definition of the signal-to-disturbance ratio. The algorithm iteratively optimises the coefficients of the prototype filters of the analysis and synthesis filter-banks using iteratively adapted weighting factors. We show that all iteration steps represent quadratic constrained optimization problems, and propose an efficient implementation. A numerical example shows that the signal-to-disturbance ratio of the output-signal is highly improved compared to that of standard designs.

## 1. INTRODUCTION

Complex-modulated (DFT) subband-coder filter-banks (filter-bank Pairs: FBP) are widely used in multirate signal processing for uniform spectral decomposition [4, 9], where power consumption and, hence, computation is crucial; e.g. mobile systems, hearing aids, etc. In addition, both a specified output-signal quality (signal-to-disturbance ratio) and the subband-signal quality must strictly be maintained. To avoid excessive FIR filter lengths, suitable oversampling of the subband-signals by an integer factor is applied [2]. Since the output-signal degradation caused by aliasing and imaging is exclusively controlled by the stopband attenuation of the FBP prototype filters, extensive subband-signal amplification generally leads to a significantly decreased signal quality [2]. In this contribution, the design of non-recursive DFT FBP is revisited, which provides high output-signal quality even with extensive subband-signal amplification.

In the past, many attempts have been made to design oversampling, complex-modulated filter-bank prototype filter pairs with high output-signal quality for a uniform amplification pattern [3, 8]. In [3], based on a two-criteria objective function, subband (denoted by inband) aliasing and the FBP output disturbance (so called residual aliasing) are concurrently minimised in the frame of an iterative design procedure: The coefficients of the prototype filters of the analysis and the synthesis filter-bank, AFB and SFB, are alternately optimised and allow for controlling the distortion function at each frequency point. In a similar design approach [8], the main focus is on minimising the FBP output disturbance by alternately optimising the AFB and SFB prototype filters, respectively. In a different approach [1, 6] (and partially published in [2]), the mechanisms of the aliasing and imaging disturbances of oversampling DFT FBP are thoroughly investigated. As a result, an overall specification of the AFB and SFB prototype filters with frequency-dependent stopband requirements are derived to maintain a prescribed minimum value of the signal-to-disturbance ratio of the output-signal that is essentially independent of subband-signal manipulation.

This contribution is organised as follows: In section 2, we give a brief description of oversampling complex-modulated FBP, along with the definition of the frequency-dependent signal-to-disturbance ratio. Next, in section 3, we discuss the basic idea of the proposed approach and assess the expected performance. Subsequently, in section 4, the objective functions and constraints are derived. The details and an efficient implementation of the optimisation procedure are presented. An illustrative example is shown in section 5, followed by concluding remarks.

## 2. OVERSAMPLING COMPLEX-MODULATED FIR FILTER-BANK PAIRS

For an oversampling complex-modulated  $I$ -channel filter-bank with additional subband-signal amplification  $\xi_l, l \in \{0, \dots, I-1\}$ , as shown in fig. 1, the AFB filters are derived from a common real-valued FIR prototype filter [4, 9]

$$H(z_i) = \sum_{k=0}^{N_h-1} h(k) \cdot z_i^{-k} = \mathbf{h}^T \cdot \boldsymbol{\phi}_h(z_i), \quad (1)$$

by modulation (frequency shifting) according to

$$\underline{H}_l(z_i) = H(z_i W_l^I), \quad l \in \{0, \dots, I-1\}, \quad (2)$$

where  $W_l = e^{-j2\pi/I}$ ,  $\mathbf{h} = [h(0), h(1), \dots, h(N_h-1)]^T$  contains the  $N_h$  coefficients of the impulse response and  $\boldsymbol{\phi}_h(z_i) = [1, z_i^{-1}, \dots, z_i^{-(N_h-1)}]^T$  comprises the associated delays. Similarly, all SFB filters are derived from a common real-valued FIR prototype filter

$$G(z_i) = \sum_{k=0}^{N_g-1} g(k) \cdot z_i^{-k} = \mathbf{g}^T \cdot \boldsymbol{\phi}_g(z_i), \quad (3)$$

according to

$$\underline{G}_l(z_i) = G(z_i W_l^I), \quad l \in \{0, \dots, I-1\}, \quad (4)$$

with the coefficient vector  $\mathbf{g} = [g(0), g(1), \dots, g(N_g-1)]^T$  and the delay vector  $\boldsymbol{\phi}_g(z_i) = [1, z_i^{-1}, \dots, z_i^{-(N_g-1)}]^T$ .

The real-valued input signal  $x(n) \xrightarrow{z^T} X(z_i)$  in fig. 1 is simultaneously passed through all AFB channel filters  $\underline{H}_l(z_i), l \in \{0, \dots, I-1\}$  and subsequently downsampled by a factor of  $M$ , yielding the subband-signals

$$\underline{X}_l(z_n) = \frac{1}{M} \sum_{k=0}^{M-1} \underline{H}_l(z_n^{1/M} W_M^k) \cdot X(z_n^{1/M} W_M^k), \quad (5)$$

where  $l \in \{0, \dots, I-1\}$ , and the alias component representation is used [4, 9]. Next, each subband-signal is individually amplified by the factor  $\xi_l, l \in \{0, \dots, I-1\}$ , yielding

$$\underline{Y}_l(z_n) = \xi_l \cdot \underline{X}_l(z_n), \quad l \in \{0, 1, \dots, I-1\}. \quad (6)$$

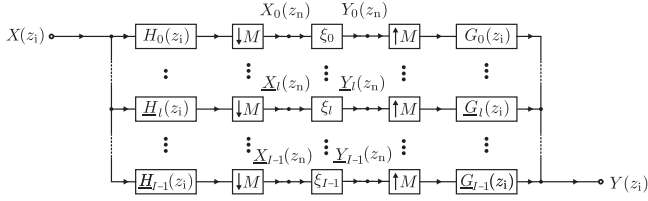


Figure 1: Uniform Oversampling filter-bank pair, oversampling factor  $\mathcal{O} = I/M \in \mathbb{N}$

In the SFB, the amplified and  $M$ -fold upsampled subband-signals  $\underline{Y}_l(z_i^M) = \underline{Y}_l(z_n)$  are combined to form the  $z$ -domain output-signal representation [4]

$$Y(z_i) = \sum_{l=0}^{I-1} \underline{G}_l(z_i) \cdot \underline{Y}_l(z_i^M). \quad (7)$$

Inserting the upsampled form of (5) into (6) and (7), we obtain

$$Y(z_i) = \underbrace{\frac{1}{M} \sum_{l=0}^{I-1} \xi_l \cdot \underline{H}_l(z_i) \cdot \underline{G}_l(z_i)}_{\mathcal{S}(z_i)} \cdot X(z_i) + \underbrace{\frac{1}{M} \sum_{k=1}^{M-1} \left[ \sum_{l=0}^{I-1} \xi_l \cdot \underline{H}_l(z_i W_M^k) \cdot \underline{G}_l(z_i) \right]}_{\mathcal{N}(z_i)} \cdot X(z_i W_M^k). \quad (8)$$

Obviously, the output-signal representation  $Y(z_i)$  depends not only on the input signal  $X(z_i)$ , but also on the  $M-1$  modulation components  $X(z_i W_M^k)$ ,  $k \in \{1, \dots, M-1\}$ . These modulation components are induced by the sample rate conversion and are considered as undesired multirate disturbance (aliasing & imaging). In (8) all these multirate components are combined to  $\mathcal{N}(z_i)$ . The remaining part  $\mathcal{S}(z_i)$  represents the desired transfer characteristics of the filter-bank pair, e.g. in case of hearing aids, it is supposed to reflect the amplification pattern applied to the subband-signals. The corresponding transfer function of the zeroth ( $k=0$ ) modulation component is considered as the distortion function [4, 9]

$$F_{\text{dist}}(z_i) = \frac{1}{M} \left[ \sum_{l=0}^{I-1} \xi_l \cdot H(z_i W_M^l) \cdot G(z_i W_M^l) \right]. \quad (9)$$

Inserting (1) and (3) into (9) for the case of a uniform amplification pattern  $\xi_l = 1$ ,  $l \in \{0, \dots, I-1\}$ , we obtain the matrix representation

$$F_{\text{dist}}(z_i) = \mathbf{h}^T \cdot \Psi(z_i) \cdot \mathbf{g}, \quad (10)$$

with the  $N_h \times N_g$  matrix

$$\Psi(z_i) = \frac{1}{M} \sum_{l=0}^{I-1} \phi_{\mathbf{h}}(z_i W_M^l) \cdot \phi_{\mathbf{g}}^T(z_i W_M^l). \quad (11)$$

### Performance Measure

In order to determine the potential of a FBP design algorithm to reduce the undesired disturbance  $\mathcal{N}(z_i)$  for any subband-signal amplification pattern, we introduce the frequency-dependent signal-to-disturbance ratio (SDR) for all of the  $I$  subbands of the FBP

$$\frac{\text{SDR}_{\kappa}}{\text{dB}} = 10 \cdot \log_{10} \left( \frac{\int_{\kappa \cdot \frac{2\pi}{T}}^{(\kappa+1) \cdot \frac{2\pi}{T}} \left| \sum_{l=0}^{I-1} \xi_l \cdot \underline{H}_l(e^{j\Omega}) \cdot \underline{G}_l(e^{j\Omega}) \right|^2 d\Omega}{\sum_{k=1}^{M-1} \int_{\kappa \cdot \frac{2\pi}{T}}^{(\kappa+1) \cdot \frac{2\pi}{T}} \left| \sum_{l=0}^{I-1} \xi_l \cdot \underline{H}_l(e^{j\Omega} W_M^k) \cdot \underline{G}_l(e^{j\Omega}) \right|^2 d\Omega} \right), \quad (12)$$

where  $\kappa \in \{0, \dots, I-1\}$ . It can be shown that for a white-noise input signal the integrand in the numerator corresponds to the power spectral density function (PSD) of  $\mathcal{S}(e^{j\Omega})$  and the integrand in the denominator corresponds to the mean PSD of  $\mathcal{N}(z_i)$ .

### 3. BASIC APPROACH

The basic idea of the optimisation procedure is explained best with an example. We choose a realistic FBP with  $I = 64$  channels and downsampling/interpolation factor  $M = 16$ . Hence the oversampling factor  $\mathcal{O} = I/M = 4$ . We use the symmetric 'ski-slope' subband-signal amplification pattern [2]

$$\xi_l = \begin{cases} 1, & l \leq 10 \\ 10^{\frac{l-10}{8} \cdot \frac{60}{20}}, & 10 \leq l \leq 17 \\ 10^{\frac{60}{20} = 1000}, & 18 \leq l \leq 32 \end{cases} \quad (13)$$

Next, we design FBP prototype filters according to the method in [8]. The passband- and stopband-edge frequencies of the corresponding filter-bank prototype filters are  $\Omega_p = \pi/64$  and  $\Omega_s = \pi/16$ , respectively [8]. We require  $\min_{\kappa \in \{0, \dots, I-1\}} \{\text{SDR}_{\kappa}\} \geq 50\text{dB}$

for the above amplification pattern. The smallest prototype filter lengths of the AFB and SFB which meet this demand are  $N_h = 99$  and  $N_g = 112$ .

Fig. 2 shows the logarithmic frequency-dependent SDR (12) for the 'ski-slope' amplification pattern along with the frequency-dependent SDR (grey colored) for a uniform amplification pattern, which exhibits a constant value of 88.7dB.

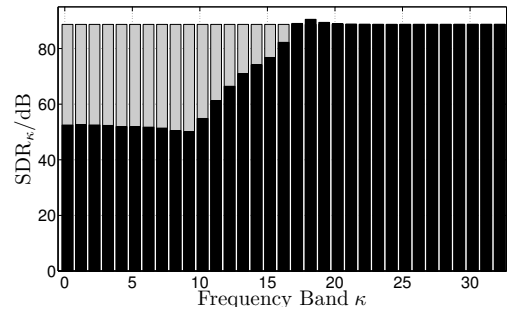


Figure 2: Frequency-dependent SDR for  $N_h = 99$  and  $N_g = 112$ .

Since the method in [8] minimizes the non-linear disturbance  $\mathcal{N}(z_i)$  for the case of a uniform amplification pattern  $\xi_l = \text{const.}, \forall l \in \{0, \dots, I-1\}$ , consequently for the 'ski-slope' amplification pattern (13) the disturbance is not minimal and the frequency-dependent SDR drops from approximately 90dB down to 50dB<sup>1</sup>. In order to obtain the minimal disturbance for the 'ski-slope' amplification pattern the exceeding frequency bands with up to 90dB have to be relieved thus creating scope for the improvement of the weak ones. This is the basic idea of the proposed method. As a result the minimum value of 50dB might be obtained with significantly lower prototype filter lengths.

This idea is based upon the unproven assumption, that among all prototype filter pairs of identical length the one with  $\text{SDR}_{\kappa} \approx \text{const.}, \forall \kappa \in \{0, \dots, I-1\}$  exhibits the largest  $\min_{\kappa \in \{0, \dots, I-1\}} \{\text{SDR}_{\kappa}\}$ .

### 4. ITERATIVE FILTER-BANK DESIGN

Next, we explore the means to implement this basic idea. To this end we examine the definition of the frequency-dependent SDR according to (12). We see that the integrand in the numerator corresponds to  $|F_{\text{dist}}(e^{j\Omega})|^2$ , which however is fully determined by the

<sup>1</sup>Similar drop-off of the frequency-dependent SDR is also observed with prototype filters obtained according to the method in [3].

transfer characteristics of the filter-bank [7]. As a consequence only the denominator of (12) has an impact on the frequency-dependent SDR

$$\sum_{\kappa=1}^{M-1} \int_{\kappa \cdot \frac{2\pi}{J}}^{(\kappa+1) \cdot \frac{2\pi}{J}} \left| \sum_{l=0}^{I-1} \xi_l \cdot \underline{H}_l(e^{j\Omega} W_M^k) \cdot \underline{G}_l(e^{j\Omega}) \right|^2 d\Omega, \quad (14)$$

where  $\kappa \in \{0, \dots, I-1\}$ . In order to implement the basic idea the above expression has to be increased in magnitude for the overloaded frequency bands (or the corresponding indices  $\kappa$  respectively), such that the SDR is reduced in these frequency bands. Similarly, (14) is decreased for all indices  $\kappa$  which correspond to the weak frequency bands, thus improving the SDR.

Since the integrand in the denominator corresponds to the mean PSD of  $\mathcal{N}(z_i)$  in (8), the presented approach implies a shaping of the disturbance (equivalent to noise shaping). According to the above assumption, the optimum is reached when  $\text{SDR}_\kappa \approx \text{const.}, \forall \kappa \in \{0, \dots, I-1\}$ , which is met only if both integrands (hence the PSD) are identical except for a constant scaling factor.

In the following an iterative approach to the implementation of the basic idea is presented. It consists of two constrained optimizations subproblems, alternatingly applied for the design of the AFB prototype filter and the SFB prototype filter, respectively. The objective functions maintain a high output-signal quality, whilst the distortion function (9) is controlled by the constraints.

#### 4.1 AFB prototype filter

We define the following single objective functions

$$\alpha_{\mathbf{h}}(\eta) = \sum_{\kappa=1}^{M-1} \sum_{l=0}^{I-1} \int_{\eta \cdot \frac{2\pi}{J}}^{(\eta+1) \cdot \frac{2\pi}{J}} \left| \xi_l \cdot \underline{H}_l(e^{j\Omega} W_M^k) \cdot \underline{G}_l(e^{j\Omega}) \right|^2 d\Omega, \quad (15)$$

where  $\eta \in \{0, \dots, J-1\}$ , which are subsequently combined using weighting factors  $w_\eta > 0$

$$\tilde{\alpha}_{\mathbf{h}} = \sum_{\eta=0}^{J-1} w_\eta \cdot \alpha_{\mathbf{h}}(\eta). \quad (16)$$

The weighting factors are iteratively adapted, thus allowing for reshaping of the frequency-dependent SDR (12). The single objective functions  $\alpha_{\mathbf{h}}(\eta)$  are upper estimates of (14) applying the triangle inequality<sup>2</sup>. Furthermore for each frequency band  $\kappa$  in (14) we define  $a \in \mathbb{N}$  separate objective functions, which yield a total number of  $\mathcal{J} = a \cdot I$  objective functions. The higher resolution is not mandatory, however empirically better results are obtained for this reason.

Next we show that (16) is a positive definite quadratic function with respect to  $\mathbf{h} = [h(0), \dots, h(N_{\mathbf{h}}-1)]^T$ . To this end the integrand in (15) is rewritten using (1) and (3)

$$\begin{aligned} \left| \underline{H}_l(e^{j\Omega} W_M^k) \cdot \underline{G}_l(e^{j\Omega}) \right|^2 &= \left| \mathbf{h}^T \cdot \Phi_{l,k}(e^{j\Omega}) \cdot \mathbf{g} \right|^2 \\ &= \mathbf{h}^T \cdot \Phi_{l,k}(e^{j\Omega}) \cdot \mathbf{g} \cdot \mathbf{g}^T \cdot \Phi_{l,k}^H(e^{j\Omega}) \cdot \mathbf{h}, \end{aligned} \quad (17)$$

with the  $N_{\mathbf{h}} \times N_{\mathbf{g}}$  matrix

$$\Phi_{l,k}(e^{j\Omega}) = \phi_{\mathbf{h}}(e^{j\Omega} W_I^l W_M^k) \cdot \phi_{\mathbf{g}}^T(e^{j\Omega} W_I^l). \quad (18)$$

Next we insert (17) into (15) obtaining

$$\alpha_{\mathbf{h}}(\eta) = \mathbf{h}^T \cdot \mathbf{A}(\eta) \cdot \mathbf{h}, \quad (19)$$

<sup>2</sup>The original formulation (14) leads to an ill-conditioned quadratic optimisation problem.

with the Hermitian  $N_{\mathbf{h}} \times N_{\mathbf{h}}$  matrix

$$\mathbf{A}(\eta) = \sum_{\kappa=1}^{M-1} \sum_{l=0}^{I-1} \xi_l^2 \int_{\eta \cdot \frac{2\pi}{J}}^{(\eta+1) \cdot \frac{2\pi}{J}} \Phi_{l,k}(e^{j\Omega}) \cdot \mathbf{g} \cdot \mathbf{g}^T \cdot \Phi_{l,k}^H(e^{j\Omega}) d\Omega. \quad (20)$$

Matrix  $\mathbf{A}(\eta)$  depends on the SFB prototype filter  $\mathbf{g}$  of the preceding optimisation step<sup>3</sup>. Therefore both optimisation steps can not be run independently. A comparison of (15) and (19) shows for  $\mathbf{g} \neq \mathbf{0} \in \mathbb{R}^{N_{\mathbf{g}}}$  that matrix  $\mathbf{A}(\eta)$  is positive definite

$$\begin{aligned} \sum_{\kappa=1}^{M-1} \sum_{l=0}^{I-1} \int_{\eta \cdot \frac{2\pi}{J}}^{(\eta+1) \cdot \frac{2\pi}{J}} \left| \xi_l \cdot \underline{H}_l(e^{j\Omega} W_M^k) \cdot \underline{G}_l(e^{j\Omega}) \right|^2 d\Omega = \\ \mathbf{h}^T \cdot \mathbf{A}(\eta) \cdot \mathbf{h} > 0, \end{aligned} \quad (21)$$

since an equality sign on the right side implies  $\eta = 0, \dots, J-1$

$$\xi_l^2 \cdot \left| \underline{H}_l(e^{j\Omega} W_M^k) \right|^2 \cdot \left| \underline{G}_l(e^{j\Omega}) \right|^2 = 0, \forall \Omega \in [\eta, \eta+1] \cdot \frac{2\pi}{J}, \quad (22)$$

which is only satisfied for  $\mathbf{h} = \mathbf{0} \in \mathbb{R}^{N_{\mathbf{h}}}$  due to the finite amount of zeros for FIR filters [4]. Inserting (19) into the objective function (16), we obtain finally

$$\tilde{\alpha}_{\mathbf{h}} = \mathbf{h}^T \cdot \tilde{\mathbf{A}} \cdot \mathbf{h}, \quad (23)$$

with the matrix

$$\tilde{\mathbf{A}} = \sum_{\eta=0}^{J-1} w_\eta \cdot \mathbf{A}(\eta). \quad (24)$$

Matrix (24) is positive definite according to (21) and  $w_\eta > 0$ .

The elements of  $\tilde{\mathbf{A}}$  are given by [5]

$$\left[ \tilde{\mathbf{A}} \right]_{\mathbf{v}, \mu} = \left( w_{\mathbf{M}}(\mathbf{v} - \mu) - \frac{1}{M} \right) \cdot \left( \Theta_1(\mathbf{v}, \mu) + \Theta_2(\mathbf{v}, \mu) \right), \quad (25)$$

where  $\mathbf{v}, \mu \in \{0, \dots, N_{\mathbf{h}}-1\}$  and  $w_{\mathbf{M}}(k) = \sum_{l=0}^{M-1} W_M^{-k \cdot l}$  represents the comb sequence [9]. Furthermore the two expressions in (25) are given by

$$\Theta_1(\mathbf{v}, \mu) = \sum_{k=-(N_{\mathbf{h}}+N_{\mathbf{g}}-2)}^{N_{\mathbf{h}}+N_{\mathbf{g}}-2} r_{\text{gg}}^E(k - \mathbf{v} + \mu) \cdot \Xi(k), \quad (26)$$

and

$$\Theta_2(\mathbf{v}, \mu) = \sum_{k=-(N_{\mathbf{h}}+N_{\mathbf{g}}-2)}^{N_{\mathbf{h}}+N_{\mathbf{g}}-2} r_{\text{gg}}^E(k + \mathbf{v} - \mu) \cdot \Xi(k), \quad (27)$$

where  $r_{\text{gg}}^E(k) = g^*(-k) * g(k)$  represents the deterministic autocorrelation function [9] and

$$\Xi(k) = \frac{\pi M}{J} \sum_{l=0}^{I-1} \sum_{\eta=0}^{J-1} \xi_l^2 \cdot w_\eta \cdot W_I^{-l \cdot k} \cdot W_J^{k \cdot (\eta + \frac{1}{2})} \cdot \text{si}\left(k \cdot \frac{\pi}{J}\right). \quad (28)$$

Furthermore matrix  $\tilde{\mathbf{A}}$  has Toeplitz structure which allows for an efficient implementation.

<sup>3</sup>In the first iteration a suitable initial filter has to be chosen.

#### 4.2 SFB prototype filter

Similarly to the previous optimisation step, we define for each frequency band  $\kappa$  in (14) again  $a \in \mathbb{N}$  separate objective functions

$$\beta_{\mathbf{g}}(\eta) = \sum_{k=1}^{M-1} \sum_{l=0}^{I-1} \int_{\eta \cdot \frac{2\pi}{T}}^{(\eta+1) \cdot \frac{2\pi}{T}} \left| \xi_l \cdot \underline{H}_l(e^{j\Omega} W_M^k) \cdot \underline{G}_l(e^{j\Omega}) \right|^2 d\Omega, \quad (29)$$

where  $\eta \in \{0, \dots, \mathcal{J}-1\}$ , which are combined using the same weighting factors  $w_\eta > 0$  as in (16)

$$\tilde{\beta}_{\mathbf{g}} = \sum_{\eta=0}^{\mathcal{J}-1} w_\eta \cdot \beta_{\mathbf{g}}(\eta). \quad (30)$$

As in section 4.1, it can be shown that (30) is a positive definite quadratic function with respect to  $\mathbf{g} = [g(0), \dots, g(N_{\mathbf{g}}-1)]^T$  and can be written as

$$\tilde{\beta}_{\mathbf{g}} = \mathbf{g}^T \cdot \tilde{\mathbf{B}} \cdot \mathbf{g}. \quad (31)$$

The elements of  $\tilde{\mathbf{B}}$  are given by

$$\left[ \tilde{\mathbf{B}} \right]_{\nu, \mu} = \Lambda_1(\nu, \mu) + \Lambda_2(\nu, \mu), \quad (32)$$

where  $\nu, \mu \in \{0, \dots, N_{\mathbf{g}}-1\}$  and the two expressions are given by

$$\Lambda_1(\nu, \mu) = \sum_{(k)} \left( w_M(k-\nu+\mu) - \frac{1}{M} \right) \cdot r_{\text{hh}}^E(k-\nu+\mu) \cdot \Xi(k), \quad (33)$$

and

$$\Lambda_2(\nu, \mu) = \sum_{(k)} \left( w_M(k+\nu-\mu) - \frac{1}{M} \right) \cdot r_{\text{hh}}^E(k+\nu-\mu) \cdot \Xi(k), \quad (34)$$

where  $\Xi(k)$  is defined by (28) and  $k = -(N_{\mathbf{h}} + N_{\mathbf{g}} - 2), \dots, N_{\mathbf{h}} + N_{\mathbf{g}} - 2$ . Again matrix  $\tilde{\mathbf{B}}$  has Toeplitz structure.

#### 4.3 Design Constraints

The constraints must guarantee the desired transfer characteristics of the filter-bank which are determined by the distortion function (9). The numerator of (12) consists of the squared magnitude of the distortion function and is therefore controlled by the constraints. According to [7] it is sufficient to design the prototypes of the FBP under the condition that the resulting distortion function (9) is approximately a linear-phase allpass function for  $\xi_l = 1, \forall l \in \{0, \dots, I-1\}$  in order to obtain the desired transfer characteristics for subband-signal amplification. Hence for every step of optimisation the constraints are defined according to [3]

$$\left| F_{\text{dist}}(e^{j\Omega}) - e^{-j\tau_{\mathbf{g}}^{\text{des}} \cdot \Omega} \right| \leq \varepsilon, \quad \Omega \in \left[ 0, \frac{\pi}{T} \right], \quad (35)$$

where the restricted frequency range exploits the  $\frac{2\pi}{T}$ -periodicity of the distortion function and  $\tau_{\mathbf{g}}^{\text{des}} = c \cdot T, c \in \mathbb{N}$  is the desired delay [6]. With the real rotation theorem [3] it is possible to estimate the upper bound of a complex value by its real part. Employing this theorem to (35) and using (10) we get

$$\mathbf{h}^T \cdot \text{Re} \left\{ \Psi(e^{j\Omega}) \cdot e^{-j\theta} \right\} \cdot \mathbf{g} \leq \cos(\theta + \tau_{\mathbf{g}}^{\text{des}} \cdot \Omega) + \varepsilon, \quad (36)$$

where  $\Omega \in [0, \frac{\pi}{T}]$  and  $\theta \in [0, 2\pi)$ . The elements of the  $N_{\mathbf{h}} \times N_{\mathbf{g}}$  matrix are given by

$$\left[ \text{Re} \left\{ \Psi(e^{j\Omega}) \cdot e^{-j\theta} \right\} \right]_{\nu, \mu} = \frac{I}{M} \cdot w_I(\mu + \nu) \cdot \cos((\mu + \nu) \cdot \Omega + \theta), \quad (37)$$

where  $\nu \in \{0, \dots, N_{\mathbf{h}}-1\}$  and  $\mu \in \{0, \dots, N_{\mathbf{g}}-1\}$ . In the implementation of the design procedure  $\Omega$  and  $\theta$  are discretised [3, 8].

#### 4.4 Algorithm

Finally, the presented positive definite quadratic objective functions and the linear constraints (with respect to both  $\mathbf{h}$  and  $\mathbf{g}$ ) are combined, yielding convex quadratic optimization problems. The iteration counter is denoted by  $i$ .

##### AFB prototype filter

This optimization step consists of the objective function (16) and the constraints (36).

$$\begin{aligned} \min_{\mathbf{h}} \tilde{\alpha}_{\mathbf{h}} &= \sum_{\eta=0}^{\mathcal{J}-1} w_\eta^{(i)} \cdot \alpha_{\mathbf{h}}(\eta) = \mathbf{h}^T \cdot \tilde{\mathbf{A}}^{(i)} \cdot \mathbf{h} \\ \mathbf{g}^T \cdot \text{Re} \left\{ \Psi^T(e^{j\Omega}) \cdot e^{-j\theta} \right\} \cdot \mathbf{h} &\leq \cos(\theta + \tau_{\mathbf{g}}^{\text{des}} \cdot \Omega) + \varepsilon, \end{aligned} \quad (38)$$

where  $\Omega \in [0, \frac{\pi}{T}]$  and  $\theta \in [0, 2\pi)$ . The AFB prototype filter  $\mathbf{h}$  is optimized, while the SFB prototype filter  $\mathbf{g}$  of the preceding optimisation step is fixed.

##### SFB prototype filter

This optimization step consists of the objective function (30) and the constraints (36).

$$\begin{aligned} \min_{\mathbf{g}} \tilde{\beta}_{\mathbf{g}} &= \sum_{\eta=0}^{\mathcal{J}-1} w_\eta^{(i)} \cdot \beta_{\mathbf{g}}(\eta) = \mathbf{g}^T \cdot \tilde{\mathbf{B}}^{(i)} \cdot \mathbf{g} \\ \mathbf{h}^T \cdot \text{Re} \left\{ \Psi(e^{j\Omega}) \cdot e^{-j\theta} \right\} \cdot \mathbf{g} &\leq \cos(\theta + \tau_{\mathbf{g}}^{\text{des}} \cdot \Omega) + \varepsilon, \end{aligned} \quad (39)$$

where  $\Omega \in [0, \frac{\pi}{T}]$  and  $\theta \in [0, 2\pi)$ . Similarly, the SFB prototype filter  $\mathbf{g}$  is optimized, while the AFB prototype filter  $\mathbf{h}$  of the preceding optimisation step is fixed.

##### Multiplicative Update

The weights  $w_\eta^{(i+1)}, \eta = 0, \dots, \mathcal{J}-1$ , in (38) and (39) are updated after each iteration. For their calculation we use the frequency-dependent SDR (12) modified for higher resolution<sup>4</sup>  $\text{SNR}_\eta^{(i)}/\text{dB}, \eta \in \{0, \dots, \mathcal{J}\}$ . The reciprocal value of the upper expression allows for the correct weighting of the frequency bands according to the basic idea presented in section 3. However the simple reciprocal value fails to converge. We have found empirically that by using the additional scaling factor

$$c(i) = \min_{\forall \eta \in \{0, \dots, \mathcal{J}-1\}} \left\{ \text{SNR}_\eta^{(i)} \right\}, \quad (40)$$

and decreasing the number of updated frequency bands using the floor function

$$w_\eta^{(i+1)} = w_\eta^{(i)} \cdot \left( 1 + p_A \cdot \left\lfloor p_N \cdot \frac{c(i)}{\text{SNR}_\eta^{(i)}} \right\rfloor \right), \quad (41)$$

in most cases convergence is achieved. The non-negative parameter  $p_A$  in (41) controls the amplitude of the multiplicative update and therefore influences the speed of convergence. However a large value often decreases the stability of convergence. Parameter  $p_N > 1$  allows for controlling the number of frequency bands used for the update. If  $p_N = 1$  only the index of the smallest value of  $\text{SNR}_\eta^{(i)}/\text{dB}, \eta \in \{0, \dots, \mathcal{J}\}$ , is considered. We observed a strong convergence for the values  $p_A = 0.3$  and  $p_N = 1.05$ .

<sup>4</sup>To this end in the integration limits of (12) we replace  $I$  by  $\mathcal{J}$ .

### Exit Condition

In order to exit the iterative algorithm in case of convergence we use the following exit condition with (40) and  $q \in \mathbb{N}$

$$|c(i) - c(i-1)| < 10^{-q}. \quad (42)$$

### Flow Chart

Fig. 3 shows the flow diagram of the algorithm.

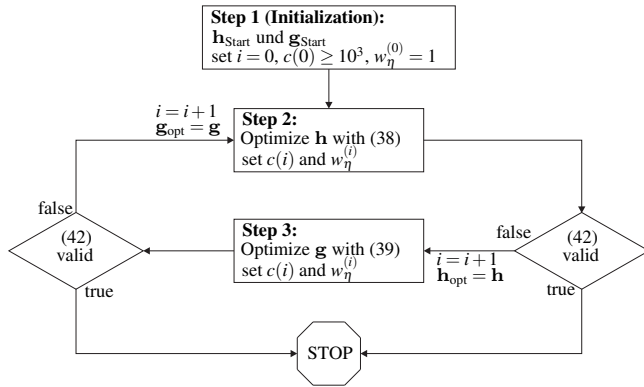


Figure 3: Flow chart

## 5. DESIGN EXAMPLE

The following design result is a solution for a FBP with the same parameters as in section 3. The lengths of the filters of the AFB and SFB are set to  $N_h = 63$  and  $N_g = 67$ . The constraint (35) of the distortion function is chosen to  $\varepsilon = 0.1$ . The parameters in (41) are  $p_A = 0.35$  and  $p_N = 1.051$ . We use  $a = 8$  objective functions (15) and (29) for each frequency band  $\kappa$  in (14). Furthermore, the desired group delay is set to  $\tau_g^{\text{des}} = I = 64$ . The number of iterations needed for the design is  $i = 160$ .

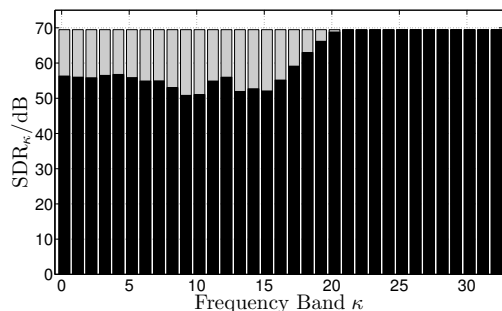


Figure 4: Frequency-dependent SDR for  $N_h = 63$  and  $N_g = 67$ .

First we look at the frequency-dependent SDR according to (12) and require a minimum value of 50dB. Fig. 4 shows the logarithmic frequency-dependent SDR for the 'ski-slope' amplification pattern (13) along with the frequency-dependent SDR (grey colored) for a uniform amplification pattern, which exhibits a constant value of 69.5dB. We observe a drop down of the frequency-dependent SDR similar to that in fig. 2 however of a much smaller difference. The minimum value is given by 50.8dB. Hence, the FBP meets the above requirement. As to the prototype filter lengths these results are a drastic improvement compared to the prototype filter pair used in section 3. Moreover both pairs exhibit approximately the same quality of distortion function and overall group delay. Finally, we want to mention that both magnitude responses of the designed prototype filter pair remarkably resemble Nyquist( $M$ ) filters ( $M$ -th band

filters [4]) with interlaced stopband domains of higher and lower rejection (i.e. don't care regions), where  $M$  represents the decimation/interpolation factor, see also [1].

## 6. CONCLUSION

We have proposed a novel iterative approach to the design of oversampling uniform DFT filter-bank pairs (FBP) of the SBC type with extensive subband-signal amplification that guarantees high output-signal quality (signal-to-disturbance ratio) despite rather small prototype filter lengths. In view of extensive subband-signal manipulation (e.g. in hearing aid applications), solely the magnitude responses of the AFB and SFB are matched, whilst aliasing compensation is not exploited.

Design examples show that the prototype filter lengths are drastically reduced by using the proposed iterative algorithm compared to existing methods applied to the numerical examples, thus guaranteeing minimal computational load of the FBP. Furthermore the advantage of the proposed approach compared to [6] is that it does not require sophisticated specifications of the stopbands and due to the inherently higher resolution thus allowing for significantly smaller prototype filter lengths.

For the proposed parameter values in (41) we have observed a strong and fast convergence of the algorithm with an average number of iterations of 200. However, in order to obtain the best possible results for given prototype filter lengths the two parameters in (41) have to be adjusted thoroughly. Furthermore, in some cases, a poor adjustment can cause convergence problems, therefore a maximum number of iterations has to be implemented.

In future research, the convergence of the algorithm will be analyzed mathematically and improvements of the empirical weighting update are expected.

## REFERENCES

- [1] D. Alfsmann and H. G. Gockler. Frequency-domain magnitude constraints for oversampling complex-modulated NPR filter bank system design ensuring prescribed signal-to-distortion ratio. In *Electronics Letters*, volume 46, 2010.
- [2] D. Alfsmann, H. G. Gockler, and T. Kurbiel. Filter Banks for Hearing Aids Applying Subband Amplification: A Comparison of Different Specification and Design Approaches. In *Europ. Sign. Process. Conf.*, Glasgow, Scotland, 2009.
- [3] H. H. Dam, S. Nordholm, A. Cantoni, and J. M. de Haan. Iterative method for the design of DFT filter bank. In *IEEE Trans. Circuits Syst. II*, volume 51, pages 581–586, 2004.
- [4] Heinz G. Gockler and Alexandra Groth. *Multiratenysteme*. Schlembach Fachverlag, Willburgstetten, 2004.
- [5] T. Kurbiel. *Optimierung und Analyse überabtastrer komplex-modulierter SBC-Filterbänke mit individuell verstärkten Teilbandsignalen*. PhD thesis, Ruhr-Universität Bochum, Germany, 2010.
- [6] T. Kurbiel, H. G. Gockler, and D. Alfsmann. A novel approach to the design of oversampling low-delay complex-modulated filter bank pairs. In *J. Advances Sign. Process.*, 2009. Article ID 692861.
- [7] T. Kurbiel, H. G. Gockler, and D. Alfsmann. Oversampling complex-modulated digital filter bank pairs suitable for extensive subband-signal amplification. In *Europ. Sign. Process. Conf.*, Glasgow, Scotland, 2009.
- [8] C. Stöcker, T. Kurbiel, D. Alfsmann, and H. G. Gockler. A novel approach to the design of oversampling complex-modulated digital filter banks. In *Europ. Sign. Process. Conf.*, Glasgow, Scotland, 2009.
- [9] P. P. Vaidyanathan. *Multirate Systems and Filter Banks*. Prentice Hall, Englewood Cliffs, NJ, 1993.